Cyclic Voltammetric studies of Mg_2SnO_4 nanoparticles and its Energy harvesting Applications

G. Karthikaselvi[1], S. Sivaranjani[1], S.R. M. Jony[2], S. Muruganantham[3], N.N. Shafeera[4]A. Ayeshamariam[4*]and M. Ismail Fathima[5]

[1]Department of Physics, St. Antony's College of Arts and Science for Women, Thamaraipadi, Dindigul, Tamil Nadu

[2]Department of Physics, Pavendar Bharathidasan College of Arts and Science, Mathur, (Affiliated to Bharathidasan University, Thiruchirappalli), Tamil Nadu, India

[3]Department of Physics, National College, (Affiliated to Bharathidasan University, Thiruchirappalli) Tamil Nadu, India

[4]Department of Physics, Khadir Mohideen College (Affiliated to Bharathidasan University, Thiruchirappalli), Adirampattinam – 614 701, Tamil Nadu, India.*

[5]Department of Physics, Sethu Institute of Technology, Pullor, Kariyapatti, 626 115, Tamil Nadu, India.

Email: ayeshamariamkmc@gmail.com

Abstract: A perfume spray pyrolysis method has been used for fabricating nanosized Mg_2SnO_4.A perfume spray pyrolysis approach has been used for making Mg_2SnO_4 in nanoscale form. X-ray diffraction (XRD), fourier transform infrared spectroscopy (FT-IR), transmission spectroscopy (UV), and scanning electron microscopy (SEM) are used to analyse the structure and morphology of the samples as-prepared. According to the findings, the crystals also form in a cubic and polycrystalline structure. The direct band gap energy of the powder synthesised at 300°C, which had the maximum optical transmittivity (>80%), was 3.67 eV. The powder manufactured at 300 °C had a measured sheet resistance and resistivity of 2.06 x 10^7 cm. Also, cyclic voltammetry was utilised to examine the samples' electrochemical characteristics. The oxidation-reduction peaks' intensities are observed to rise, but their positions and forms do not change, further indicating the stability of the electrode and the potential of Mg_2SnO_4 as an electrode material, super capacitor component, and energy-harvesting component.

Keywords: Mg_2SnO_4 nanoparticles, Spray pyrolysis method, photochemical Studies.

Introduction

Magnesium stannate (**Mg_2SnO_4**) is the most significant stannate-based material because of its excellent electrical conductivity and high-power density. Magnesium stannate is also taken into account as an alternative anode material in Li-ion batteries due to the enormous lithium-ion capacities at low potentials, as well as the fact that they are pollution-free, easily available sources of raw materials, and inexpensive. However, a battery's performance is also influenced by the active materials' crystallite size and shape in addition to its structure. [1]

A few of the developed processes for producing metal stannate NPs include co-precipitation, solid state reaction, wet chemical approach, self-heat sustained route, and hydrothermal method. The hydrothermal approach is a very practical method for producing homogenous nanoparticles with superior shape under ambient conditions, low temperature reactions, and high purity. Mg_2SnO_4, on the other hand, is primarily made via the self-heat-sustained (SHS) method and the traditional solid-state reaction (SSR) method. [2]. The high calcination temperatures 12,00°C and 16,00°C for SSR and SHS, respectively have a number of downsides, including high energy consumption, higher device standards, and the production of powders with large particle sizes [3]. Wet chemical techniques, such as the flux approach, peroxide precursor route, and polymeric precursor method, are developed to solve these drawbacks. All of these approaches, however, take a lot of time and need difficult pre-treatment procedures as well as harsh reaction conditions. A streamlined method of creating Mg_2SnO_4, is widely desired in order to reduce its drawbacks and expand its possible applications [4]. In this study, we looked at how the synthetic Mg2SnO4 made using the pyrolysis process of perfume spray performed structurally, morphologically, and electrochemically.

Experimental

Numerous applications of oxide materials include thermal barrier coatings, nuclear fuels, electrical conductors, and sensors, all of which can be impacted by stoichiometric alterations on the nanoscale scale. Atom probe tomography can be used to spatially quantify the oxygen to metal ratio at the nanoscale scale and characterise the precise chemical distribution of particular species. Yet, measurement distortions from laser-material interactions can be present when analyzing oxides with an atom probe [5]. In this study, two oxide materials with similar crystal structures and

important industrial applications tin oxide doped with magnesium oxide—are examined. It was discovered that their electronic structure, optical properties, heat transfer abilities, and oxide stability have a significant impact on how they behave during spray pyrolysis, changing their observed stoichiometry, with thermal conductance and thermodynamic stability being significant contributors. [6]

Doped tin oxide the structure, formation and development process, and surface morphology of magnesium oxide powder produced by simple co-precipitation have all been studied.

Table 1. Experimental condition of (Mg_2SnO_4) nanoparticles

Spray parameters	**Values**
quantity of the precursor	0.15 M
Precursor spray volume	50 ml
Solvent	90% Ethanol + 10% TEG
Temperature of the substrate	400-600°C
Spray amount	5 ml/min
Gas carrier pressure	0.4 kg/cm^2
Temperature of the nozzle substrate	30 cm

Results and discussion

X-Ray diffraction (XRD)

The diffractogram of the precursor Mg_2SnO_4 material is shown in Figure 1. The measured peaks for the 73-1625 Mg_2SnO_4 sample are given in Table 2 and compared to its standard data. It should be noted that the planes (111), (311), (222), and (422) correspond to the maxima for nanoparticles that were annealed at 300°C for two hours. It is concluded that the material confirms its hexagonal form either by

increasing the annealing temperature or annealing duration. However, there was a plane for all annealed films (111). The remaining peaks could be caused by the SnO2-doped metal oxide MgO. When the precursor was obtained by the co-precipitation process, it means that the precursor was oxidised at a temperature of about 300ºC. The diffraction angle peak varies depending on the length of the annealing process for all XRD patterns. It demonstrates how annealing time duration in an atmospheric setting tends to modify the crystallinity of the powder. Some of the peaks in the aforementioned patterns are those of the binary metal oxide compound as opposed to the ternary complex. It might be caused by a change in physical and chemical characteristics such density, crystal bonding, and some thermal characteristics [7].

The noticed association between the degrees of (111) preferred orientation and the deposition temperature can be attributed to molecules migrating onto the growing surface. During nucleation, MgO is anticipated to reach a favoured orientation (200) with a lower energy configuration. The absorbed Mg and O atoms were easily able to move to equilibrium atomic locations on the surface due to their greater mobility at a higher substrate temperature. Specifically, Mg_2SnO_4's energetically stable (111) plane.[8]. Thus, (111) preferred orientation dominates when the substrate temperature is ideal for packing the atoms densely and with the fewest defects. A stable (200) preferred layer is expected to finally form as a result of the substrate's thermal energy acting as a source of migratory energy for the surface atoms.

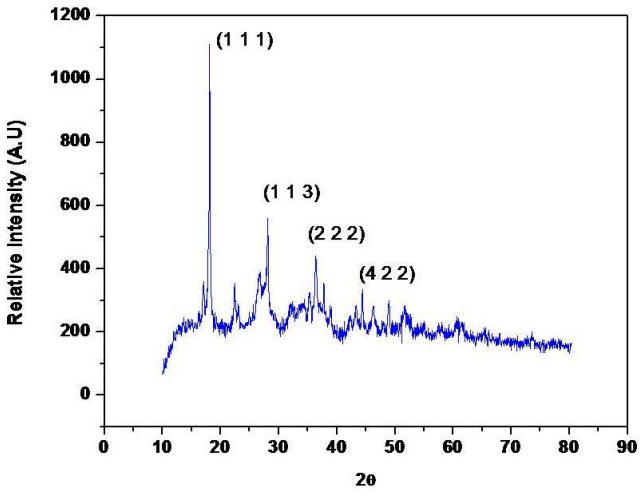

Figure 1 XRD studies of Mg_2 SnO_4

The crystallite size 'D' of MgO for the (111) and (113) diffraction peaks was calculated using Scherrer's formula. [9]:

$$D = \frac{K\lambda}{\cos\theta\sqrt{\beta^2 - \beta_0^2}}$$

where K=0.94, is the integral peak width caused by instrumental broadening, 0 is the Bragg's diffraction angle of the corresponding XRD peak, and is the wavelength of the incident x-ray radiation (1.542 for CuK). This knowledge makes it possible to calculate the dislocation density () from = 1/D2, the micro strain () from = (/Dsin)-(/tan), and the number of crystallites per unit area (N), all of which may be used to determine the composition of the produced MgO powder. Table 2 displays the estimated values for the measured line-widths and the other variables discussed previously.

where K=0.94, is the Bragg's diffraction angle of the corresponding XRD peak, is the intrinsic full width at half maximum of the peak, 0 is the integral peak width induced by instrumental broadening, and is the wavelength of incident x-ray radiation (1.542 for CuK). With the aid of this information, it is possible to determine the dislocation density (δ) from = $1/D^2$, the micro strain (ε),and the number of crystallites per unit area (N), which will help to clarify the composition of the MgO powder produced. The estimated values for the measured line-widths and the other above-mentioned values are shown in Table 2.

Table 2 Structural data of the particle and its calculation

Reflecting plane <hkl>	Lattice constant (Å)		Theta (2θ)		Crystallite size, D (nm)	Strain, ε 10^{-3}	hkl planes	Intensity
	Observed	JCPDS Standards	Observed	Standard				

111	4.8998	4.9877	18.115	18.1048	76.21	-0.0176	111	100.0
311	2.5973	2.6047	34.775	34.5338	15.91	-0.3867	311	13.39
222	2.5408	2.4938	36.256	35.3261	22.62	0.0188	222	16.76
422	1.7713	1.7634	52.105	51.5984	1.042	0.0067	422	8.85

In the current study, Mg_2SnO_4 was employed to create nanomaterials utilizing the co-precipitation method. Magnesium tin oxide was transformed into tiny new particles.

FTIR spectroscopy

Information on phase composition and the type of bonding between oxygen and metal ions can be found in the results of FTIR spectroscopy. The FTIR spectrum of Mg_2SnO_4 heated to 300 °C in Figure 2 shows the complete thermal conversion of the precursor into oxide. There are five transmission bands with frequencies of 607 cm^{-1} (v_1), 633 cm^{-1} (v_2), 766 cm^{-1} (v_3), 1091 cm^{-1} (v_4), and 3566 cm^{-1} (v_5). $Mg(OH)_2$ and hydrogen-bonded hydroxyl groups are responsible for the very small peak that can be seen at 3499 cm^{-1} [9]. The water deformation band and the C-O stretching absorption in the bicarbonate and carbonate ions, respectively, are responsible for the big peaks at 1664 cm^{-1} and 766 cm^{-1} [10]. The most likely source of these pollutants, according to the co-precipitation method, is the precursor, solvent, or environmental exposure. It is well known that Mg_2SnO_4 surfaces chemisorbed water and carbon dioxide molecules when exposed to the atmosphere. Therefore, it is likely that a little amount of contamination was integrated during the film's exposure to the ambient environment. Peak Mg-O absorption is thought to occur between 400 and 600 $cm^{-1.}$ The longitudinal optical (LO) phonon modes in the MgO lattice are responsible for the prominent peaks at 607 and 582 cm^{-1}. This shows that the structure of Mg_2SnO_4 is dominated by the vibrations Mg-O-Mg and O-Sn-O. Mg_2SnO_4 has a wave number of 607 cm-1, whereas pure ionic magnesium oxide has a wave number of 582 cm^{-1} [11]. The intensities of Mg-O-Mg and O-Sn-O both increase as the calcination temperature rises. The O-H vibration strength also dropped at this time, possibly as a result of water molecules evaporating. These findings support the XRD result and highlight the significance of the calcination temperature. The longitudinal optical (LO) phonon

modes of the MgO lattice are responsible for the strong peaks at 607 and 582 $cm^{-1.}$ Mg_2SnO_4 has a wave number of 607 cm^{-1}, whereas the wave number of Mg-O desorption in pure ionic magnesium oxide is 582 cm^{-1}. [11].

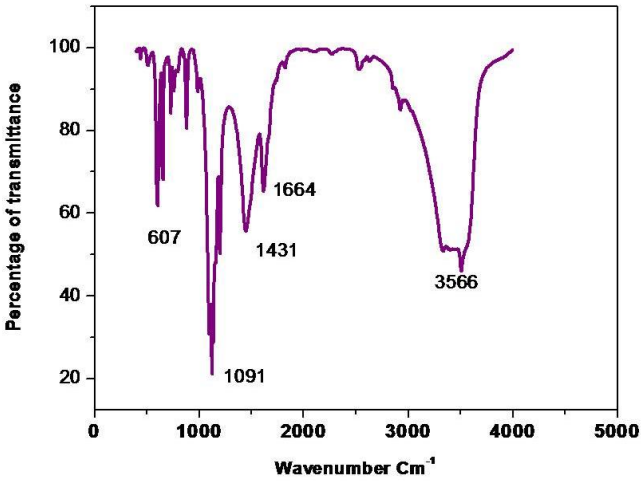

Figure 2 FTIR Analysis of Mg_2SnO_4 Nanoparticles

Optical absorption studies

The wavelength range of the optical absorption spectra was 200–1500 nm. The optical transmittance curve for Mg_2SnO_4 nanoparticles as a function of wavelength is depicted in Figure.3a at an annealing temperature of 300°C. It was found that the films' absorption coefficient was in the neighbourhood of 104 cm^{-1}. It is discovered that when the substrate temperature rises, the percentage transmission (%T) value in the visible zone rises.. For MgO powder manufactured at 300 °C, lower transmission values and maximum transmission behavior are observed. The increased optical characteristics and well-adhered, crystalline structure of the powder across the coated zone that were attained as a result of uniform oxidation and improved lattice configurations are what are responsible for the increase in percent T. [12].

To determine the type of optical transition in these samples, the optical data were evaluated using classical equations. $\alpha = \alpha_o \dfrac{(h\nu - E_g)^n}{h\nu}$

where E_g stands for the distance between the top of the valence band and the bottom of the conduction band, "h" stands for the photon energy, and "n" is a constant.For a permitted direct transfer, n = 1/2, while for a permitted indirect transition, n equals 2.

Figure 3 displays the plots of (h)2 against h for all of the samples that were deposited. Plot characteristics point to a direct inter-band transfer. The calculation of band gap energy results from extrapolating straight-line parts to zero absorption co-efficient . at 300 °C, samples have a band gap energy (Eg) of 3.67 eV [13].

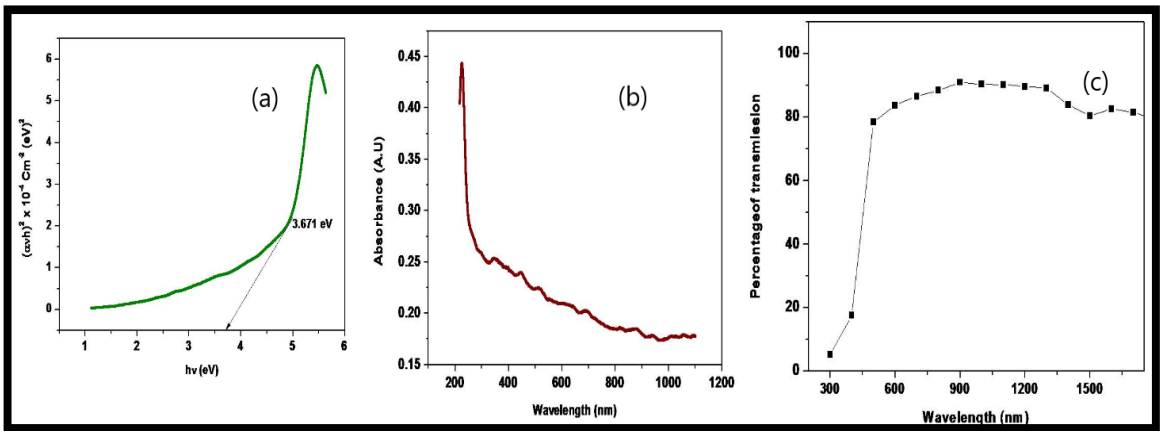

Figure 3. (a) Bandgap Analysis (b) Absorbance (c) Transmittance Analysis of Mg_2SnO_4 Nanoparticles

Absorption Coefficient $\alpha = 2.303\log(\frac{A}{T})$

Where T = % of Transmission and A = Absorbance value

Extinction Coefficient $k = \frac{\alpha\lambda}{4\pi}$

Refractive index $= \frac{(1+R)}{(1-R)} + \sqrt{\frac{(1+R)^2}{(1-R)^2}} - \sqrt{(1+k^2}$

Particle size $= \frac{\lambda_1\lambda_2}{2(\lambda_1 n_2 - \lambda_2 n_1)}$ nm

The following properties of the electronic structure are mostly responsible for the perturbation of the energy gap between the conduction band and valence band in this instance [14]. Additionally, the magnesium, which are located near the oxygen vacancies, undergo electron redistributions. [15].

SEM and EDAX analysis

SEM and EDAX examinations of Mg_2SnO_4's surface showed its surface morphology and element composition, which is evident in Fig. 7. The Mg_2SnO_4' NPs are depicted in this picture to have a consistent size distribution and an irregular cubic shape. In table 3, the elemental composition of the prepared NPs was displayed. The formation of Mg_2SnO_4' NPs and the absence of impurities demonstrate the purity of the samples. The preparation circumstances and calcination temperature may have a considerable impact on the size and morphology of the Mg_2SnO_4 NPs.

Electrical properties

The structure (grain size and shape, flaws, etc.), purity (concentration of impurities absorbed and adsorbed gases, moisture, etc.), and preparation conditions all have a significant impact on the electrical transport characteristics of Mg_2SnO_4 powder. The two-probe method allowed for direct measurement of the films' ressitivities. By applying a known potential across the sample's end contacts, a high-precision electrometer was used to quantify the currents. As opposed to 7.98 x 10^{12} /cm for films generated at 500 °C, the sheet resistance of Mg_2SnO_4 films made at 600 °C was on the order of 10^{13} /cm at room temperature. The equivalent resistivity values are 2.12x10^6 cm and 2.06 cm x 10^7 cm. [16]

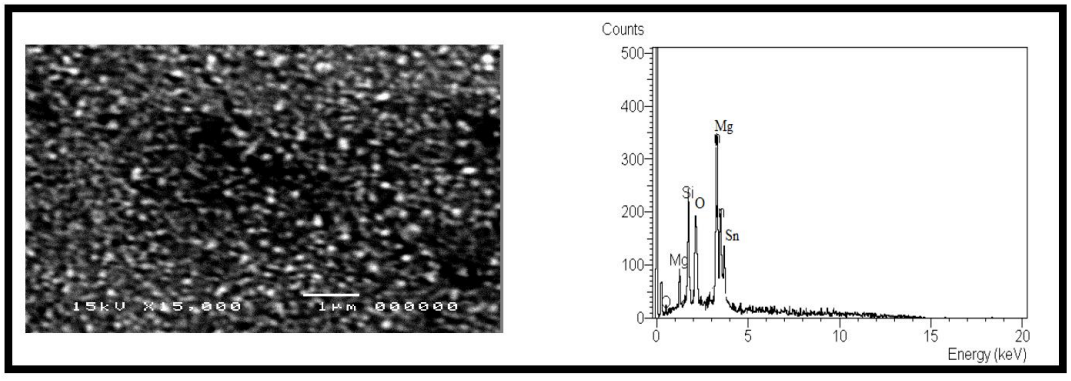

Figure 7 SEM and EDAX Analysis of Mg_2SnO_4 Nanoparticles

AC Conductivity measurement

To comprehend the conduction mechanism in these materials, measurements of AC conductivity in insulating materials have been widely used. According to the widely held belief, localised states within the energy gap dominate the AC conductivity. Therefore, measuring AC conductivity is a potent experimental

technique to learn about the localised states. Complex impedance spectroscopy (CIS) has been used in the current work to describe the electrical processes that take place in a system when an AC signal is applied to the sample that is sandwiched between the electrodes. When presented as a complex plane plot, the output response of such an experimental measurement takes the shape of a series of semicircles that indicate the contributions to the electrical characteristics made by the bulk material, grain boundary effect, and interfacial polarisation. Therefore, the CIS approach is helpful to very readily distinguish the effects resulting from each component in a polycrystalline sample. Data from impedance measurements on a material includes both reactive (imaginary part) and resistive (actual part) elements. Any formalism, including complex impedance, complex admittance, complex permittivity, and complex modules, can be used to represent it in a complex plane plot [17].

Table 3 EDAX Analysis of Mg_2SnO_4 Nanoparticles

Element	Intensity (A.U)	Elemental composition	Atomic %	Atomic %	Atomic %
O K	0640	1.53	4.01	1.02	22.08
Mg K	0953	1.63	3.42	0.39	10.62
Sn L	1075	1.51	92.57	1.06	67.03

Additionally, the complex impedance spectrum's semicircular arc peak gives the material's relaxation frequency as well as its corresponding resistance and capacitance values. A material's bulk conductivity (dc), a thermally activated process that follows Arrhenius behaviour, can be calculated using the bulk resistance (Rb), which is determined from a complicated impedance spectrum. The relation can be used to compute the bulk conductivity.,

$$\sigma_{dc} = \frac{1}{R_b} \frac{d}{A}$$

where 'A' denotes the sample's area and 'd' denotes the thickness.

According to the relationship, the AC conductivity of the material characterizing the frequency-dependent behavior of the conduction process may be assessed. $\sigma_{AC} = \omega \varepsilon' \varepsilon_o \tan \delta$

where tan δ denotes the dielectric loss,'denotes permittivity, and 'o denotes permittivity in vacuum.

Films were sandwiched between two electrodes for AC measurements. The silicon substrate served as the bottom electrode, while the top electrode was formed by thermally evaporating aluminium onto the surface of MgO powder in a predetermined area. Direct measurements of the impedance Z, capacitance C, and phase were made using a programmed LCZ bridge. The equation was used to compute the total conductivity. [18] $\sigma_{tot}(\omega) = \frac{d}{ZA}$

where 'A' is the sample's cross-sectional area and 'd' is the film's thickness. From the equation, the dielectric constant (') was derived.

$$\varepsilon' = \frac{Cd}{A\varepsilon_o}$$

where "'ε_o " represents the permittivity of empty space.The equation was used to compute the dielectric loss (ε)

$$\varepsilon'' = \varepsilon' \tan\delta$$

where, δ = 90-ϕ and 'ϕ' is the phase angle.

The Nyquist plot of $MgSnO_3$ powdered particles

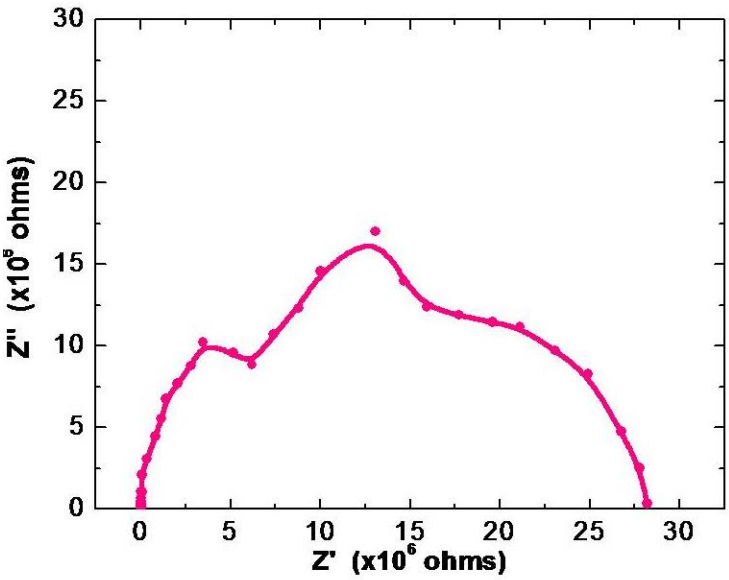

Figure. 8. The Nyquist plot of $MgSnO_3$ powdered particles

Mg_2SnO_4 powder's AC conductivity was assessed between the ranges of 40 and 100,000 hertz and 30 and 90^oC, respectively.

Cyclic voltmeter studies

Using CV measurement, the electrochemical performance of the sample was evaluated at different scan rates in a potential window between -1.5 and -2.5 V $ms^{-1.}$ In order to evaluate the enhanced electro-chemical performance in a three electrode system, the Mg_2SnO_4 NPs were tested as a working electrode (WE), and the CV curve for the calcinated Mg_2SnO_4 electrode was recorded at various temperatures ranging from 20°C to 100°C.

Figure displays the results that were achieved. The first-discharge sweep at 20°C and the discharge sweeps at 100°C are very different from one another, similar to charge-discharge profiles. It demonstrates that as the temperature rises, the sweep sharply rises. Mg_2SnO_4 is a promising candidate for electrode material and super capacitor application, according to the results of both the charge-discharge and cyclic voltammograms.

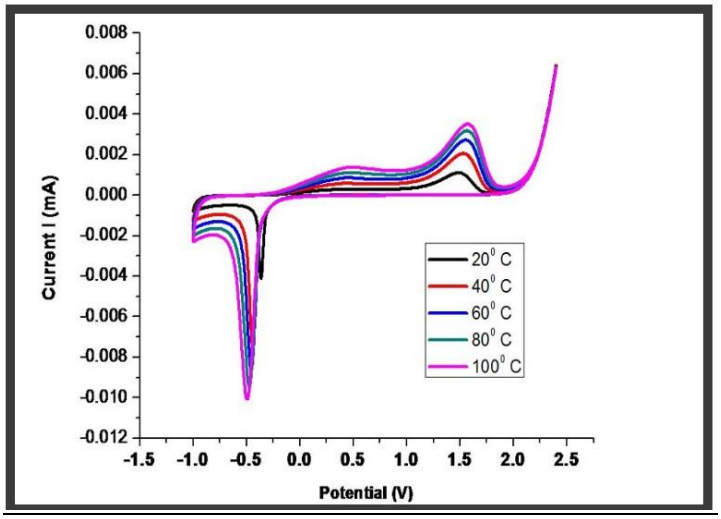

Figure 8 shows the CV curves of Mg_2SnO_4 NPs that have been calcinated up to 100 °C at various scan rates.

4. Conclusion

The spray pyrolysis method has been used to successfully create magnesium oxide powder at 300°C. The process variables were adjusted to produce crystalline films of high quality. The FTIR measurements allowed for the identification of the

Mg_2SnO_4 phase development. All of the films were transparent in the visible and IR range of radiation when the substrate temperature was increased to 300°C, with transparency greater than 80% and an associated band gap value of 3.67 eV. The resistivity of the produced films is around 107 cm^{-1}. Based on the findings of cyclic voltammetry, it is determined that Mg_2SnO_4 is a promising choice for energy harvesting applications such as electrodes and super capacitors.

References

[1]. Petnikota, S., Rotte, N.K., Reddy, M.V., Srikanth, V.V. and Chowdari, B.V., 2015. MgO-decorated few-layered graphene as an anode for Li-ion batteries. *ACS applied materials & interfaces*, *7*(4), pp.2301-2309.

[2]. He, P., Xie, Z., Chen, Y., Dong, F. and Liu, H., 2012. Co2SnO4/activated carbon composite electrode for supercapacitor. *Materials Chemistry and Physics*, *137*(2), pp.576-579.

[3]. Chauhan, N., Rawal, R., Hooda, V. and Jain, U., 2016. Electrochemical biosensor with graphene oxide nanoparticles and polypyrrole interface for the detection of bilirubin. *Rsc Advances*, *6*(68), pp.63624-63633.

[4] Shamirian, A., Edrisi, M. and Naderi, M., 2013. Synthesis, Characterization, and Optimization of Co 2 SnO 4 Nanoparticles via Co-precipitation Method. *Journal of materials engineering and performance*, *22*, pp.306-311.

[5]. Azad, A.M., 2001. Novel synthesis of high phase-purity Mg_2SnO_4 from metallic precursors via powder metallurgy route. *Materials research bulletin*, *36*(3-4), pp.755-765.

[6]. Pfaff, G., 1993. Wet chemical synthesis of BaSnO3 and Ba2SnO4 powders. *Journal of the European Ceramic Society*, *12*(2), pp.159-164.

[7]. Al-Shahrani, A.A., 2005. Sintering behavior and thermal property of Mg 2 SnO 4. *Journal of Materials Science: Materials in Electronics*, *16*, pp.193-196.

[8]. Qin, Y., Xiong, J., Zhang, W., Liu, L., Cui, Y. and Gu, H., 2015. Facile synthesis and photocatalytic performance of Mg 2 SnO 4/SnO 2 heterostructures. *Journal of Materials Science*, *50*, pp.5865-5872.

[8]. Xiao, T., Tang, Y., Jia, Z. and Feng, S., 2009. Synthesis of SnO_2/Mg_2SnO_4 nanoparticles and their electrochemical performance for use in Li-ion battery electrodes. *Electrochimica acta*, *54*(8), pp.2396-2401.

[9]. Hu, J., Zhang, Z., Zhao, M., Qin, H. and Jiang, M., 2008. Room-temperature ferromagnetism in MgO nanocrystalline powders. *Applied physics letters*, *93*(19), p.192503.

[10]. Okada, T., Naoi, T. and Yoshioka, T., 2009. Decay kinetics of luminescence and electron emission from MgO crystal powders in ac plasma display panels. *Journal of Applied Physics*, *105*(11), p.113304.

[11]. Xiao, T., Tang, Y., Jia, Z. and Feng, S., 2009. Synthesis of SnO_2/Mg_2SnO_4 nanoparticles and their electrochemical performance for use in Li-ion battery electrodes. *Electrochimica acta*, *54*(8), pp.2396-2401.

[12]. Tang, H., Cheng, C., Yu, G., Liu, H. and Chen, W., 2015. Structure and electrochemical properties of Mg_2SnO_4 nanoparticles synthesized by a facile co-precipitation method. *Materials Chemistry and Physics*, *159*, pp.167-172.

[13]. Selvakumaran, D., Manickam, A., Ravi, G., Muthusamy, G. and Seshatri, B., 2019. Improved Photocatalytic and Electrochemical Performance of Hydrothermally Synthesized Mg_2SnO_4 Nanocubes and their Effect on Loading with Activated Carbon. *Advanced Materials Proceedings*, *4*(3), pp.109-111.

[14]. Costa, J.M., Lima, L.C., Li, M.S., Santos, I.M.G., Silva, M.R.S. and Maia, A.S., 2019. Structural and photocatalytic properties of Mg_2SnO_4 spinel obtained by modified Pechini method. *Materials Letters*, *236*, pp.320-323.

[15]. Li, M., Jin, Y., Yuan, L., Wang, B., Wu, H., Hu, Y. and Wang, F., 2023. Near-Infrared Long Afterglow in Fe^{3+}-Activated Mg_2SnO_4 for Self-Sustainable Night Vision. *ACS Applied Materials & Interfaces*, *15*(10), pp.13186-13194.

[16]. Da Silva Junior, E.B., López, A., Pedro, S.S. and Sosman, L.P., 2019. Photoluminescence of Co^{2+} ions in Mg_2SnO_4 tetrahedral sites. *Optical Materials*, *95*, p.109202.

[17]. Zhang, J.C., Qin, Q.S., Yu, M.H., Zhou, H.L. and Zhou, M.J., 2011. Photoluminescence and persistent luminescence properties of non-doped and Ti4+-doped Mg2SnO4 phosphors. *Chinese Physics B*, *20*(9), p.094211.

[18]. Kebede, M.A. and Palaniyandy, N., 2019. Metal oxide-based anode materials for lithium-ion battery. *Electrochemical Devices for Energy Storage Applications*, pp.19-40.